Bifurcations and Chaotic Motions in a Two-axis Rate Gyro

Heng-Hui Chen, Ming Chang and Fu-Ping Chang

Abstract

An analysis is presented of a two-axis rate gyro mounted on a space vehicle that is spinning with uncertain angular velocity $\omega_z(t)$ about its spin of the gyro. For the non-autonomous case in which $\omega_z(t)$ is sinusoidal function, this system is a strongly nonlinear damped system subjected to parametric excitation. By varying the amplitude of sinusoidal motion, periodic and chaotic responses of this parametrically excited nonlinear system are investigated using the numerical simulation. The results, Symmetry-breaking bifurcations, period-doubling bifurcations, and chaotic behavior of the system are observed by various numerical techniques such as phase portraits, Poincaré maps, average power spectra, and Lyapunov exponents.

Key Words: Rate Gyro, Bifurcation, Chaos

Heng-Hui Chen : Associate Professor, Department of Mechnical Engineering, HIT
Ming Chang : Instructor, Department of Mechnical Engineering, HIT
Fu-Ping Chang : Instructor, Department of Mechnical Engineering, HIT

雙軸速率陀螺儀之分歧與混沌運動

陳恒輝・張　敏・張福平

摘要

本論文將對一飛行器上之雙軸速率陀螺儀作詳細動力分析，此時飛行器相對於自轉軸作$\omega_z(t)$轉動。當飛行器相對於自轉軸作簡諧轉動時，這系統爲參數激勵強非線性耗散系統，隨著系統參數變動下，系統呈現規則與混沌反應行爲。經由相軌跡、龐加萊截面、平均功率普與李雅普若夫指數等數值模擬方法來分析系統，發現隨系統參數變化，系統存在數種不同型態的解與分歧行爲如Hopf分歧、對稱分歧與倍週期分歧，並得到系統混沌行爲。

關鍵詞：速率陀螺儀、分歧、混沌

陳恒輝：本校機械工程系助理教授
張　敏：本校機械工程系講師
張福平：本校機械工程系講師

1. Introduction

A number of studies over the past few decades have shown that chaotic phenomena are observed in many physical systems that possess both non-linearity and external excitation [1]. The nonlinearity of a system, through the various system parameters, exhibits a variety of nonlinear behaviors including jump phenomenon, multiple attractors, subharmonic vibrations, symmetry breaking-bifurcations, period-doubling bifurcations, crisis and chaos [2]. In addition, a symmetry-breaking bifurcation occurring before a period-doubling bifurcation, and the appearance of chaos amidst a cascade of period-doubling bifurcations have been observed in driven damped pendulums or Duffing's oscillators by MacDonald and Räty [3]. In a gyroscopic system, a single-axis rate gyro mounted on a space vehicle free to move in various ways also exhibits complex nonlinear and chaotic motions. The nonlinear nature and chaotic motion of a single-axis rate gyro were investigated by Ge[4] when the vehicle is spinning sinusoidally with respect to the spin axis of the gyro. This system is characterized by parametric excitation and exhibits complex nonlinear phenomena in the presence of sinusoidal excitation, including subharmonic vibrations, Hopf bifurcation, symmetry-breaking bifurcations, a series of period-doubling bifurcations, and chaos.

In this paper, an analysis is presented of a two-axis rate gyro mounted on a space vehicle that is spinning with uncertain angular velocity $\omega_Z(t)$ about the spin of the gyro. For the non-autonomous case in which ω_Z is sinusoidal function, a number of numerical techniques are used to detect the existence of symmetry-breaking bifurcations, period- doubling bifurcations, and chaos of the parametrically excited nonlinear system. The natures of the periodic and chaotic motions are shown in phase plane diagrams, Poincaré maps and average

power spectra. The qualitative bifurcation diagrams, parametric diagrams and quantitative Lyapunov exponents in parametric space are also computed to determine the values of bifurcation points as well as chaos onset.

2. Equations of Motion

We consider the model of a two-axis rate gyro mounted on a space vehicle as shown in Fig. 1. Let X, Y, Z be a set of axes attached to the platform and ξ, η, ζ be gimbal axes. The rotor is mounted in the inner gimbal that can turn about axis X with rotational angle θ. The rotation of the inner gimbal is resisted by torsional spring and damping torques defined by $T_c(=k_1\theta)$, $d_1\dot{\theta}$ respectively. The outer gimbal rotates about the axis Y with rotational angleϕ, and motion about this axis is also resisted by torsional spring and damping torques defined by $k_2\phi$, $d_2\dot{\phi}$, respectively. Using Largrange's equation [5], the differential equations of a two-axis gyro with feedback control was derived as follows;

$$(A+A_1)[\ddot{\theta}-\omega_X\sin\phi+\omega_Z\cos\phi)\dot{\phi}+(\dot{\omega}_X\cos\phi-\dot{\omega}_Z\sin\phi)]-(A+B_1-C_1)\omega_\eta\omega_\zeta-(-\omega_\eta)H_c+d_1\dot{\theta}+k_1\theta=0, \quad (1)$$

$$d/dt[(A+B_1)\omega_\eta\cos\theta-C_1\omega_\zeta\sin\theta+A_2(\dot{\phi}+\omega_Y)-\sin\theta H_c]+d_2(\dot{\phi}+\omega_Y)+k_2\phi=0, \quad (2)$$

where

$\dot{\theta}=d\theta/dt$, $\dot{\phi}=d\phi/dt$, $H_c=[C(\omega_\zeta+\dot{\psi})]=$const.,

$\omega_\xi=\dot{\theta}+(\omega_X\cos\phi-\omega_Z\sin\phi)$,

$\omega_\eta=(\dot{\phi}+\omega_Y)\cos\theta+(\omega_X\sin\phi+\omega_Z\cos\phi)\sin\theta$,

$\omega_\zeta=-(\dot{\phi}+\omega_Y)\sin\theta+(\omega_X\sin\phi+\omega_Z\cos\phi)\cos\theta$.

ω_X, ω_Y, ω_Z denote the angular velocity components of the platform along output axis X, input axis Y, and normal axis Z, respectively. A, B (= A), C and A_1, B_1, C_1 denote the moments of inertia of rotor and inner gimbal about ξ, η, and ζ, respectively. A_2 denotes the moment of inertia of the outer gimbal about axis Y.

3. Numerical Simulations and Discussion

We consider the case in which ω_Z is time-varying, $\omega_Y = 0$ and $\omega_X = 0$. The origin (θ, $\dot{\theta}$, ϕ, $\dot{\phi}$=(0,0,0,0) is an equilibrium point. However, in the

following analysis, with a harmonic input with respect to the spin axis Z, i.e., $\omega_Z = f\sin\omega_f t$, the origin becomes a hyperbolic closed orbit. The differential equations of the model can be simplified as follows:

$$\ddot{\theta} + 2\alpha_1\dot{\theta} + k\theta + \alpha_2\dot{\phi} + NF_1(\theta,\phi,\tau) = 0, \quad (3)$$

$$\ddot{\phi} + 2\beta_1\dot{\phi} + \beta_2\phi - \beta_3\dot{\theta} + NF_2(\theta,\phi,\tau) = 0 \quad (4)$$

where

k=1, $\dot{\theta}=d\theta/d\tau$, $\dot{\phi}=d\phi/d\tau$, $NF_1(\theta,\phi,\tau)$ and $NF_2(\theta,\phi,\tau)$, shown in Appendix A; $\omega_n=[k_1/(A+A_1)]^{1/2}$; frequency ratio $\omega=\omega_f/\omega_n$, the exciting frequency is close to twice the natural frequency; time scale $\tau=\omega_n t$; damping ratio $\alpha_1=d_1/[2(A+A_1)\omega_n]$, $\beta_1=d_2/[2(A+B_1+A_2)\omega_n]$; $\alpha_2=H_c/[(A+A_1)\omega_n]$, $\beta_2=k_2/[(A+B_1+A_2)\omega_n^2]$, $\beta_3=H_c/[(A+B_1+A_2)\omega_n]$.

With the input amplitude f varied, the response results are obtained by numerical integration in the phase planes, Poincaré maps, average power spectra, bifurcations and Lyapunov exponents. Hopf bifurcation occurs when the parameter f passes through 15.4, the original equilibrium point becomes unstable and a period-2T stable symmetric limit cycle for f=18 arises as shown in Fig.2, where $T=2\pi/\omega$. A system with a symmetric nonlinear function can undergo either a symmetry-breaking bifurcation for the symmetric solution of the system or a period-doubling bifurcation for the asymmetric solution of the system. When $f\approx$29.5, a symmetry-breaking bifurcation occurs. After this bifurcation, the original stable period-2T attractor becomes unstable, a pair of stable period-2T attractors arise and invert each other as shown in Fig.3 where f=31.5. As the parameter f increases further across $f\approx$32, a stable periodic orbit appears with doubling period of the original orbit, thereby indicating a period-doubling (flip) bifurcation. When the parameter is increased, a cascade of flip bifurcations occurs and leads to the onset of chaos. At $f\approx$34, the chaotic attractor abruptly disappears and a period-6T symmetric orbit appears, as shown in the phase plane and average power spectrum (Figs.2,4).

To investigate bifurcation further, a Poincaré plane was used to display the bifurcation diagram, which shows Poincaré fixed points x_p plotted against the system parameter f. The Hopf bifurcation, symmetry-breaking bifurcation, and period-doubling bifurcation are clearly shown. As the system parameter f is gradually increased through the parametric space, the bifurcation diagram obtained shows different types of bifurcations and chaos (Fig.5). The Hopf bifurcation appears at $f\approx15.4$, the symmetry-breaking bifurcation at $f\approx29.5$, and the period-doubling bifurcation at $f=32$, as observed earlier. To investigate the periodic and chaotic motions in the bifurcation diagram further, the phase planes, Poincaré maps, and power spectra are used. After a cascade of period-doubling bifurcations, the dual response becomes chaotic rather than periodic for $f=32.5$. When $f=33$, conjunction of the two inverse chaotic attractors creates a larger attractor. With the parameter increased, a large-amplitude chaotic motion appears in the phase plane, Poincaré map, and power spectrum as shown in Fig.6, where $f=36.3$. The power spectrum of a chaotic motion is a continuous board spectrum.

To confirm the chaotic dynamics, a quantitative Lyapunov-exponent spectrum was conducted. The algorithm for calculating the Lyapunov exponents was developed by Wolf et al. [6]. A spectrum of the largest Lyapunov exponent as a function of the parameter f is shown in Fig.7. As one of the Lyapunov exponents is positive, the motion is characterized as chaotic. When at least one Lyapunov exponent $\lambda_i = 0$ exists, motions are not stationary. For periodic motions, the Lyapunov exponents are non-positive and include only one zero Lyapunov exponent, while one negative exponent becomes zero when one type of periodic motion bifurcates to another.

For $f = 36.3$ the Lyapunov exponents were found to be $\lambda_1 = 0.171$, $\lambda_2 = 0$, $\lambda_3 = -0.936$, $\lambda_4 = -0.938$, $\lambda_5 = -1.534$ and the

Lyapunov dimension d_L = 2.183 was also calculated using the relation proposed by Frederickson et al. [7]:

$$d_L = j + \sum_{i=1}^{j} \lambda_i / |\lambda_{j+1}|, \quad (3)$$

where λ_1 is the largest Lyapunov exponent and j is the index of the smallest non-negative Lyapunov exponents. From the above discussion, it is evident that Lyapunov exponents are a measure of the fractal geometry of the attractor and the property of sensitivity dependence on initial conditions.

3. Conclusions

In this paper, a two-axis rate gyro with sinusoidal velocity about its spin axis Z exhibits its nonlinear characteristic for both sin, cos functions and parametric excitation when the parameter is varied. A variety of parametric studies were performed to analyze the behavior of periodic attractors routing to chaos via distinct bifurcations by using the numerical simulations. The behaviors of a symmetry-breaking precursor to period-doubling bifurcations and a cascade of period-doubling route to chaos occurred in this system. The occurrence of the chaotic motion of the full system is also detected by calculating bifurcation diagrams, power spectral diagrams and Lyapunov exponents.

4. References

1. J. GUCKENHEIMER and P. HOLMES *Nonlinear Oscillations, Dynamical Systems and Bifurcation of Vector Fields, Springer-Verlag*, New York, 1986, Chaps. 4-7.
2. K. YAGASKI, Chaos in a Pendulum with Feedback Control, 1994, Nonlinear Dynamics **6**, 125-142.
3. RÄTY J. VON BOEHM and H. M. ISOMÄKI, Absence of Inversion-Symmetric Limit Cycles of Even Periods and the Chaotic Motion of Duffing's Oscillator, 1984, *Physics Letters* **103A**, 289-292.
4. Z. M. GE and H. H. CHEN,

Bifurcations and Chaotic Motions in a Rate Gyro with a Sinusoidal Velocity about the Spin Axis, 1997, *Journal of Sound and Vibration* **200(2)**, 121-137.

5. L. MEIROVITCH, *Methods of Analytical Dynamics*. McGraw-Hill, New York, 1970.
6. A. WOLF J. B. SWIFT H. L. SWINNEY and J. A. VASTANO, Determining Lyapunov Exponents From a Time Series, 1985 *Physica* **16D**, 285-317.
7. FREDERICKSON, J. L. KAPLAN, E. D. YORKE and J. A. YORKE, The Lyapunov dimension of strange attractors, 1983 *Journal of Differential Equations* **49**, 185-207.

Nomenclature

X, Y, Z	fixed coordinate system attached to the platform
ξ, η, ζ	moving coordinate system attached to gimbal axes
θ, ϕ, ψ	Euler angles(precession angle, nutation angle, spin angle) as generalized coordinates
A, A, C	the moments of inertia of rotor about ξ, η, and ζ axes
A_1, B_1, C_1	the moments of inertia of inner gimbal about ξ, η, and ζ axes
A_2	the moment of inertia of the outer gimbal about axis Y
k_1, k_2	torsional spring coefficients with respect to the axes of rotation of the θ, ϕ angles, respectively
d_1, d_2	damping coefficients with respect to the axes of rotation of the θ, ϕ angles, respectively
$\omega_X, \omega_Y, \omega_Z$	the angular velocity components of the platform along output axis X, input axis Y, and normal axis Z, respectively
ω_n	the natural frequency of the system
ω_f	the exciting frequency of harmonic input
f	the amplitude of harmonic input
T	the period of attractors of the system

Appendix A

$$NF_1(\theta,\phi,\tau)= -(A+B_1-C_1)(-\dot{\phi}c_2\omega_{Z1}\omega_n+(-\omega_n^2\dot{\phi}^2s_1+s_1c_2^2\omega_{Z1}^2+2\dot{\phi}c_2\omega_{Z1}\omega_nc_1)c_1)/[(A+A_1)\omega_n^2]-$$
$$Hc(-\omega_n\dot{\phi}c_1-s_1c_2\omega_{Z1}+\dot{\phi}\omega_n)/\ [(A+A_1)\omega_n^2]-(\dot{\phi}c_2\omega_{Z1}\omega_n\ +s_2\omega_n\dot{\omega}_{Z1})/\omega_n^2.$$

$$NF_2(\theta,\phi,\tau)= ((s_2^2\dot{\theta}c_2\omega_{Z1}\omega_nA_2-k_2\phi s_1^2-\dot{\phi}d_2\omega_ns_1^2)C_1+(-\omega_{Z1}^2s_2A_2+\omega_{Z1}\dot{\theta}\omega_nA_2)c_2(A+A_1)+$$
$$(2C_1s_1\dot{\phi}\dot{\theta}\omega_n^2A_2-C_1s_1c_2\dot{\omega}_{Z1}\omega_nA_2+(-\omega_{Z1}\ \dot{\theta}\omega_nA_2+\omega_{Z1}^2s_2A_2)c_2C_1c_1)c_1+$$
$$(\dot{\theta}\omega_nC_1s_1^2+\ \dot{\theta}\omega_nA_2+(s_2\omega_{Z1}\ A_2-\dot{\theta}\omega_nA_2)c_1)Hc+(k_2\phi+(-s_1^2\dot{\theta}\omega_{Z1}\omega_nA_2+$$
$$s_1^2s_2\omega_{Z1}^{\ 2}A_2)c_2+\dot{\phi}d_2\omega_n+\ C_1s_1^2\dot{\theta}c_2\omega_{Z1}\ \omega_n+(-\omega_{Z1}^{\ 2}s_2+\omega_{Z1}\dot{\theta}\omega_n)c_2(A+A_1)+$$
$$(-2s_1\dot{\phi}\dot{\theta}\omega_n^2A_2+2C_1s_1\dot{\phi}\dot{\theta}\ \omega_n^2+(s_1c_2\omega_nA_2-C_1s_1c_2\omega_n)\dot{\omega}_{Z1}+(-k_2\phi+c_2\omega_{Z1}\dot{\theta}\ \omega_nA_2-$$
$$\dot{\phi}d_2\omega_n+(\omega_{Z1}^{\ 2}s_2-\omega_{Z1}\dot{\theta}\omega_n)c_2C_1)c_1)c_1+(s_2\omega_{Z1}-\dot{\theta}\ \omega_n+c_1\dot{\theta}\omega_n)\ c_1Hc+((s_1^2s_2\omega_{Z1}^2-$$
$$s_1^2\dot{\theta}\omega_{Z1}\ \omega_n)c_2+(-2s_1\dot{\phi}\dot{\theta}\omega_n^2+s_1c_2\dot{\omega}_Z\omega_n+c_2\omega_{Z1}\dot{\theta}\omega_nc_1)c_1)(A+B_1))(A+B_1))/$$
$$[((A+B_1)c_2^2+C_1s_1^2+A_2)(A+B_1+A_2)\omega_n^2]\ .$$

where $s_1=sin\theta$, $s_2=sin\phi$, $c_1=cos\theta$, $c_2=cos\phi$, etc. $\omega_{Z1}=f\sin\omega\tau$, $\omega=\omega_f/\omega_n$, $\dot{\omega}_{Z1}=d\omega_{Z1}/d\tau$.

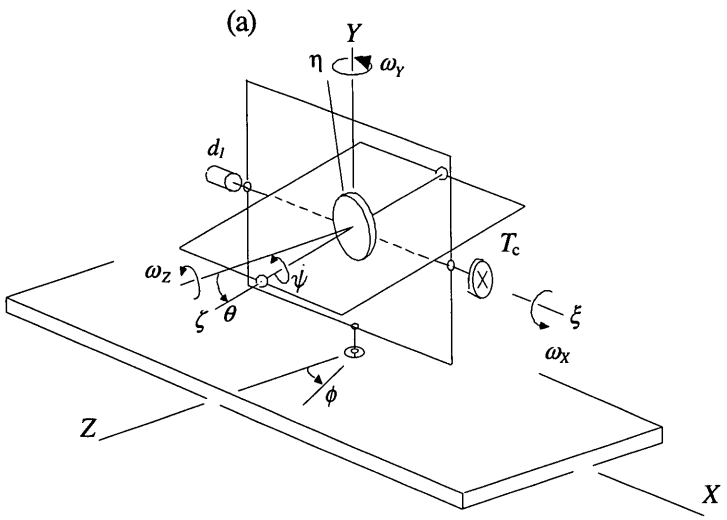

Fig.1 A two-axis rate gyro.

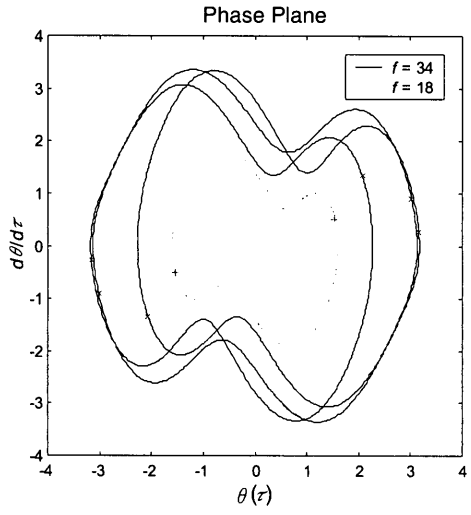

Fig.2 Two inversion-symmetric attractors: a period-2T attractor for f=18, a period-6T attractor for f= 34 where the symbols '+' and '×' indicate one period-T of $\omega_Z = f\sin\omega\tau$.

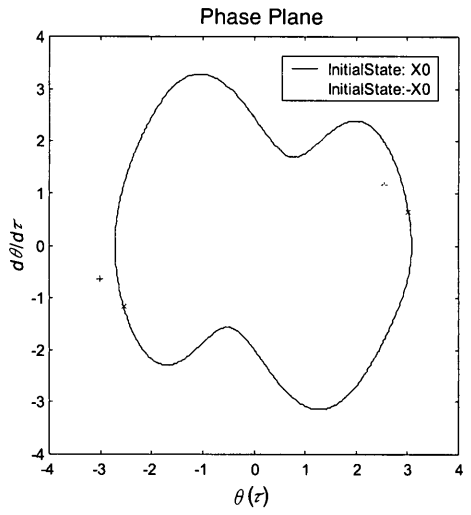

Fig.3 A dual period-2T attractor for f=31.5.

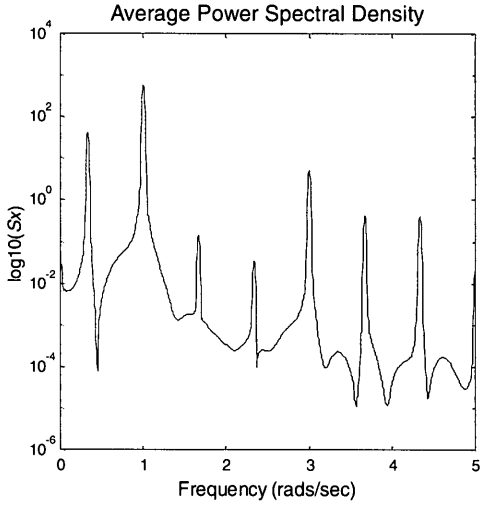

Fig.4 An average power spectrum of Fig. 2 for f=34.

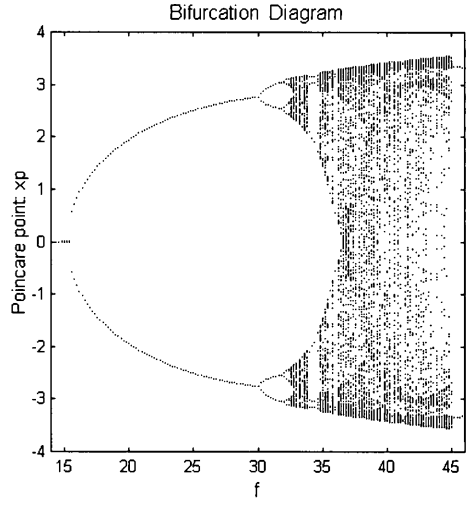

Fig.5 The bifurcation diagram.

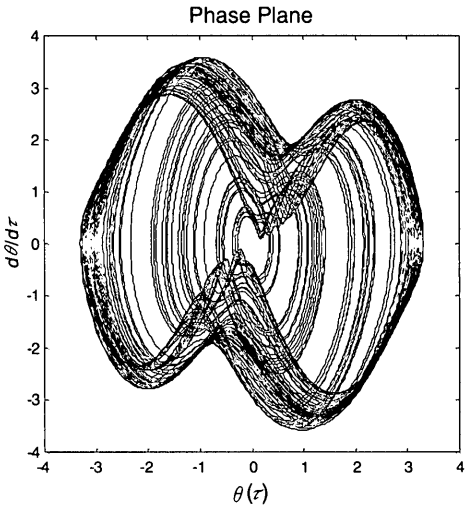

Fig.6(a) A symmetric chaotic attractor for f=36.3.

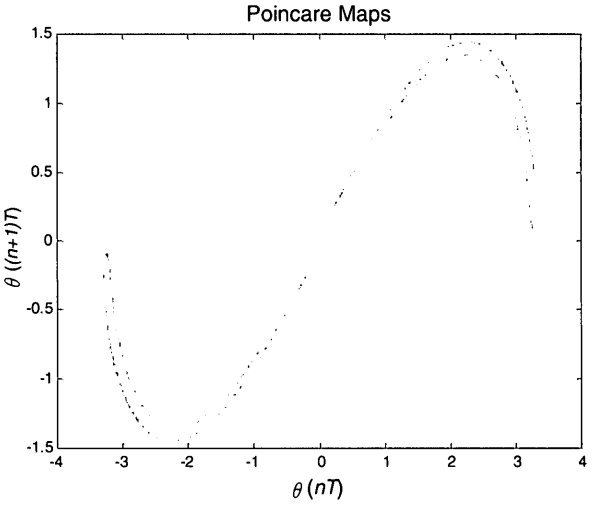

Fig.6(b) A symmetric chaotic attractor for f=36.3.

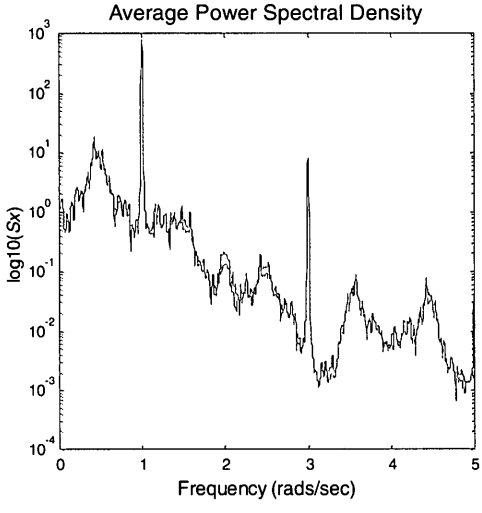

Fig.6(c) An Average power spectrum for f=36.3.

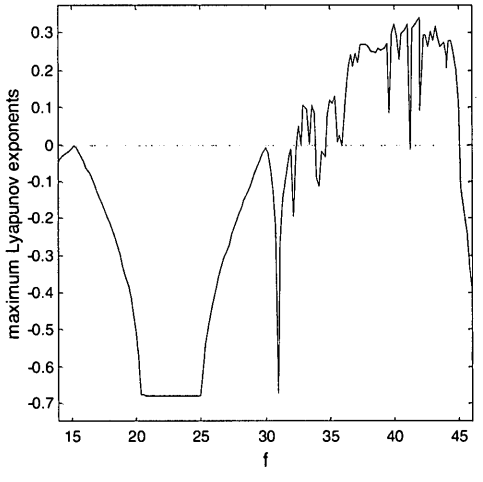

Fig.7 The largest Lyapunov exponents.